Mesoscopic Limit Cycles in Coupled Nanolasers

Mathias Marconi,[†] Fabrice Raineri,[‡] Ariel Levenson, and Alejandro M. Yacomotti[*]
Centre de Nanosciences et de Nanotechnologies, CNRS, Université Paris-Saclay, 10 Boulevard Thomas Gobert, 91120 Palaiseau, France

Julien Javaloyes
Departament de Física and IAC-3, Universitat de les Illes Balears, C/ Valldemossa km 7.5, 07122 Mallorca, Spain

Si H. Pan, Abdelkrim El Amili, and Yeshaiahu Fainman
Department of Electrical and Computer Engineering, University of California San Diego, 9500 Gilman Drive, La Jolla, California 92093, USA

(Received 25 October 2019; accepted 27 April 2020; published 27 May 2020)

Two coupled nanolasers exhibit a mode switching transition, theoretically described by mode beating limit cycle oscillations. Their decay rate is vanishingly small in the thermodynamic limit, i.e., when the spontaneous emission noise tends to zero. We provide experimental statistical evidence of mesoscopic limit cycles ($\sim 10^3$ intracavity photons). Specifically, we show that the order parameter quantifying the limit cycle amplitude can be reconstructed from the mode intensity statistics. We observe a maximum of the averaged amplitude at the mode switching, accounting for limit cycle oscillations. We finally relate this maximum to a dip of mode cross-correlations, reaching a minimum of $g_{ij}^{(2)} = 2/3$, which we show to be a mesoscopic limit. Coupled nanolasers are thus an appealing test bed for the investigation of spontaneous breaking of time translation symmetry in the presence of strong quantum fluctuations.

DOI: 10.1103/PhysRevLett.124.213602

How do quantum fluctuations affect nonequilibrium periodic orbits? This question, intimately related to the spontaneous breaking of time translation symmetry, has strongly motivated a large community of physicists in the last few years. While the spontaneous time symmetry breaking is well known in classical nonlinear dynamics as a Hopf bifurcation to limit cycle oscillations [1], its realization in the quantum world has been a subject of debate. In a seminal paper, Wilczek [2] pointed out the existence of quantum periodic motion in a time-invariant Hamiltonian, launching a new field of research known as time crystals, which are the time counterparts of spatial crystals. Since then, many efforts have been devoted to understand and implement time crystals in different domains such as condensed matter and QED systems, with particular emphasis on Floquet time crystals, which break discrete time translation symmetry (see, e.g., Ref. [3] for a review). Recently, there has been growing interest in dissipative time crystals for which the *continuous* time symmetry is spontaneously broken [4].

From a historical perspective, a paradigmatic example of nonequilibrium periodic orbits is the laser. Since the seminal works on its analogy with second order phase transitions [5–7], the laser threshold has been successfully described as a Hopf bifurcation with added noise (see [7] and references therein). In the thermodynamic limit, the intracavity photon number—which scales as the inverse of the spontaneous emission β factor—tends to infinite ([8] and Sec. VII of [26]) and the system spontaneously breaks the phase invariance [U(1) symmetry]. For a finite thermodynamic parameter (β^{-1}), however, phase diffusion restores U(1) and the coherence time becomes finite [9]. In dissipative time crystals, the problem of coherence is related to the lifetime of crystal phases, which is linked to a closure of a Liouvillian gap [4] and hence to a dissipative phase transition [10]. As in the laser case, but also in other optical systems [11,12], the persistent oscillations are associated with the spontaneous symmetry breaking since they only take place in the thermodynamic limit. A number of many body limit cycles can be classified as dissipative time crystals [4,13–15]. Limit cycles in microcavities have also been recently reported in the context of parametric instabilities [16], comb generation [17], and chaos [18]. Yet, an important open question is whether they survive in the presence of quantum fluctuations.

In this work, we propose coupled nanolasers [19–21] as test beds for limit cycles subjected to strong quantum noise—in this case due to spontaneous emission—and provide experimental evidence on the existence of limit cycles with a thousand photons inside the cavities. We explore intensity oscillations that emerge as mode beating when the coupled cavity eigenmodes operate simultaneously. Specifically, this occurs at a mode switching transition between the bonding (B) and antibonding (A) modes of a nanolaser dimer formed by two evanescently coupled

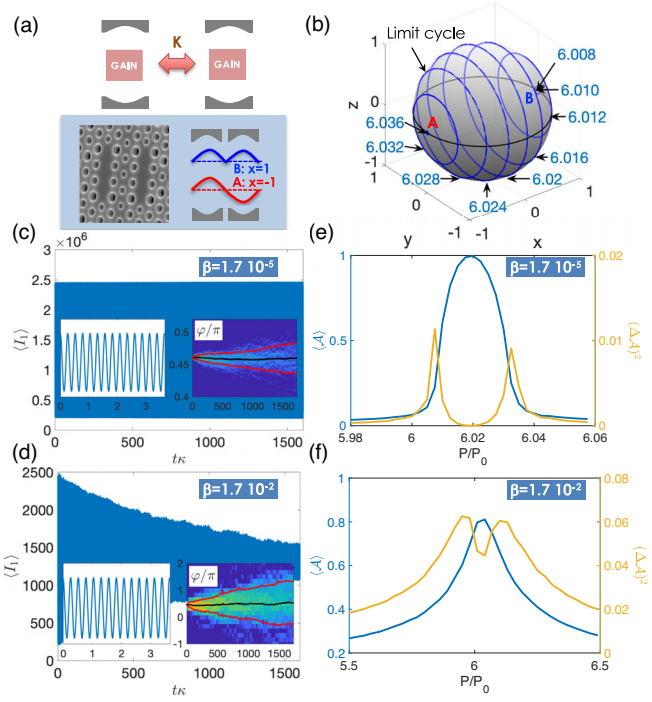

FIG. 1. Numerical simulations of mode beating limit cycles in two strongly coupled nanolasers. (a) Schematics of two evanescently coupled laser nanocavities, with coupling strength K. Bottom frame: SEM image of the fabricated indium phosphide photonic crystal cavities; right: the two eigenmodes (B: bonding, A: antibonding) are split in energy. (b) Bloch sphere showing noiseless limit cycles close to a switching point [$F_{a_{1,2}}(t) = 0$ in Eq. (1)]; blue trajectories correspond to orbits increasing pumping (P/P_0, blue labels); other parameters [Eqs. (1) and (2)] are $K = 12\kappa$, $\gamma = 0.05\kappa$, $\alpha = 7$, $\gamma_\parallel = 2.2$ GHz, $\gamma_{\rm tot} = 5$ GHz, $\kappa = 140.84$ GHz, $n_0 = 10^{18}\,{\rm cm}^{-3} \times V_a$ with $V_a = 0.016 \times 10^{-12}\,{\rm cm}^3$. (c),(d) Ensemble average of the intensity in the cavity 1 for $P/P_0 = 6.015$; the average is taken over 100 different noise realizations and the same initial conditions (see text). Insets: enlargement of a few oscillation periods (left) and histogram of the limit cycle phase φ (right, color map; average and standard deviation in black and red lines, respectively). (e),(f) Mean value and fluctuations of the order parameter as a function of the pump power P normalized to the transparency pump P_0. (c),(e) $\beta = 1.7 \times 10^{-5}$ and $V_a = 16 \times 10^{-12}\,{\rm cm}^{-3}$. (d),(f) $\beta = 0.017$ and $V_a = 0.016 \times 10^{-12}$ cm^3. Other parameters are $F_P = 1.03$ and $B = 3 \times 10^{10}$ cm^3 s^{-1}; $P_{{\rm th},B}/P_0 = 1.4496$.

photonic crystal nanocavities [Fig. 1(a)] as the pump is increased [22].

Lasers can be described by a quantum master equation [9,23]. In semiconductor laser physics, much more simplified models have been used in the past—e.g., the semiclassical theory, which neglects quantum fluctuations [8]. A more realistic description needs to incorporate spontaneous emission fluctuations produced by the semiconductor emitters such as quantum wells (QWs), which can be added to the semiclassical model in the form of Langevin noise terms. Two coupled nanolasers containing QWs can thus be modeled by the following nonlinear coupled stochastic differential equations [19,21,22]:

$$\dot{a}_{1,2} = \left(\frac{1+i\alpha}{2} G_{1,2} - \kappa\right) a_{1,2} + (\gamma + iK) a_{2,1} + F_{a_{1,2}}(t), \quad (1)$$

$$\dot{n}_{1,2} = P - \gamma_{\rm tot} n_{1,2} - G_{1,2} |a_{1,2}|^2, \quad (2)$$

where $|a_{i,j}|^2 = I_{i,j}$ and n are normalized as the photon and carrier numbers in the cavities, respectively; κ is the cavity loss rate; α the Henry factor; P the pump rate; and $\gamma_{\rm tot}$ is the total carrier recombination rate. The complex intercavity coupling constant quantifies both frequency (K) and loss (γ) splitting as a result of the evanescent coupling. $G_{1,2} = \gamma_\parallel \beta (n_{1,2} - n_0)$ is the gain, $\gamma_\parallel$ is the two-level radiative recombination rate, and n_0 the carrier number at transparency. $F_{a_i}(t)$ are Langevin noise terms accounting for spontaneous emission with rate $R_{\rm sp} = \beta F_P B n_{1,2}^2 / V_a$, where B is the bimolecular radiative recombination rate, F_P the Purcell factor, and V_a the volume of the active medium. We make the common assumption of uncorrelated (white) noise, i.e., $\langle F_\mu(t) F_\nu(t') \rangle = 2 D_{\mu\nu} \delta(t - t')$, where $D_{\mu\nu}$ are the following diffusion coefficients: $2D_{a_i a_i^*} = 2D_{a_i^* a_i} = R_{sp}$, and zero otherwise.. Importantly, the intracavity saturation intensity is $I_{\rm sat} = \gamma_{\rm tot}/\gamma_\parallel \beta$; hence β^{-1} is a good thermodynamic parameter in the sense of photon number. Three ranges can be identified: $\beta^{-1} \lesssim 10^2$, $10^2 \lesssim \beta^{-1} \lesssim 10^4$, and $\beta^{-1} \gtrsim 10^4$, corresponding to the nanoscopic, mesoscopic, and macroscopic regimes, respectively [24]. In the deep nanoscopic regime, $\beta^{-1} \lesssim 10$, Eqs. (1) and (2) are no longer valid; a full quantum model is needed, such as coupled cavity extensions of Ref. [9]. For semiconductor cavities, $\beta \sim V_a^{-1}$ [25]; hence β^{-1} is also related to the cavity size.

The two linear eigenmodes of Eq. (1) are $a_B = (a_1 + a_2)/\sqrt{2}$ and $a_A = (a_1 - a_2)/\sqrt{2}$ [Fig. 1(a)]. The dynamics of this system can be separated into two subsets of variables [21]: the total intensity and carrier number on one side, and the relative intensities and phases of the cavities on the other side, which can be recast on the Bloch sphere as $\theta = 2 \arctan(\sqrt{I_2/I_1}) \in [0, \pi]$ and $\Phi = \psi_1 - \psi_2$, where $a_j = \sqrt{I_j} \exp(i\psi_j)$. Remarkably, the x coordinate of the Bloch sphere is nothing but the mode population imbalance, $x = (I_B - I_A)/(I_B + I_A)$, where I_B and I_A are the intensities of the two eigenmodes.

Above laser threshold, the laser molecule operates in the mode with higher net gain, designed to be the B mode. A switching transition is observed from B to A modes as the pump power is ramped up due to stimulated scattering induced by carrier oscillations [22]. Indeed, Eqs. (1) and (2) show mode switching mediated by the emergence of a limit cycle in the thermodynamic limit, $\beta^{-1} \to \infty$ [22]. The B mode loses stability, expelling a limit cycle at a first Hopf bifurcation [$x = 1$, Fig. 1(b)]; these oscillations account for mode beating. The limit cycle amplitude rapidly increases up to a perfect mode beating in which both modes have the

same intensity (dual-frequency laser), and each cavity intensity experiences 100%-contrast oscillation [$x = 0$, Fig. 1(b)]. When the pump parameter is increased further, the limit cycle shrinks and coalesces at a second Hopf bifurcation, leading to a stable fixed point corresponding to the A mode [$x = -1$, Fig. 1(b)]. Note that these Hopf bifurcations break the time translation symmetry. Even though a second mode (A) turns on, no phase symmetry breaking takes place since U(1) has already been spontaneously broken at the B mode laser threshold.

The limit cycle oscillations are long-lasting solutions of the mean field limit, which is a well-known nonlinear dynamical feature: the amplitude decay rate tends to zero. In the presence of noise, fluctuations increase the decay rate. We have quantified such an effect through simulations of the Langevin equations with different β factors accounting for different "system sizes." In Figs. 1(c) and 1(d) we show the ensemble average of the cavity 1 intensity, $\langle I_1 \rangle$ for $\beta = 1.7 \times 10^{-5}$ [Fig. 1(c)] and $\beta = 1.7 \times 10^{-2}$ [Fig. 1(d)]. The initial conditions correspond to a maximum intensity in cavity 1; defining $w(t) = y(t) + iz(t) = \mathcal{A}(t) \exp[-i\Omega_{lc} t + \varphi(t)]$, where $\mathcal{A}$ and Ω_{lc} are the amplitude and frequency of the limit cycle, respectively, the initial conditions read $\varphi(t = 0) = \pi/2$. Figure 1(c) corresponds to a macroscopic cavity in which the effect of noise on the limit cycle is small, and the amplitude does not decay in the whole time window used for the calculations. The interesting situation arises in the mesoscopic regime [Fig. 1(d)]: we observe a drastic reduction in the decay time; still, the limit cycle undergoes thousands of oscillations before it dies out. The physical origin of this finite lifetime is the diffusion of $\varphi(t)$ [see insets in Figs. 1(c) and 1(d)], computed as the angle of $w(t)$ in a framework that rotates with $\Omega_{\rm lc}$, i.e., $\varphi(t) = \arg[w \exp(i\Omega_{\rm lc} t)]$. It is important to point out that the period of oscillations is $T = 2\pi/\Omega_{\rm lc} \approx \pi/K \approx 0.26$ in units of κ^{-1}, corresponding to $\Omega_{\rm lc}/2\pi \approx 545$ GHz. Such a high frequency, combined with a low output photon number, rules out any direct observation of the limit cycle. However, we show below that the limit cycle amplitude $\mathcal{A}$ can be quantified through mode intensity statistics.

By construction, the limit cycle amplitude on the Bloch sphere of Fig. 1(b) is

$$\mathcal{A} = \sqrt{1 - x^2}, \tag{3}$$

which is the natural order parameter for the formation of the limit cycle. Equation (3) states that the limit cycle vanishes for single mode operation, $x = \pm 1$, and reaches a maximum order of $\mathcal{A} = 1$ for the $x = 0$ limit cycle ($\Phi = \pi/2$) in the thermodynamic limit. In Figs. 1(e) and 1(f), we show $\langle \mathcal{A} \rangle$ and $(\Delta\mathcal{A})^2$ as a function of the pump. Clearly, $\langle \mathcal{A} \rangle$ reaches a maximum at $P/P_0 \approx 6.02$ for $\beta = 1.7 \times 10^{-5}$ [Fig. 1(e)] with two fluctuation maxima at the bifurcation points. In the nanolaser case, $\beta = 1.7 \times 10^{-2}$, $\langle \mathcal{A} \rangle$ still

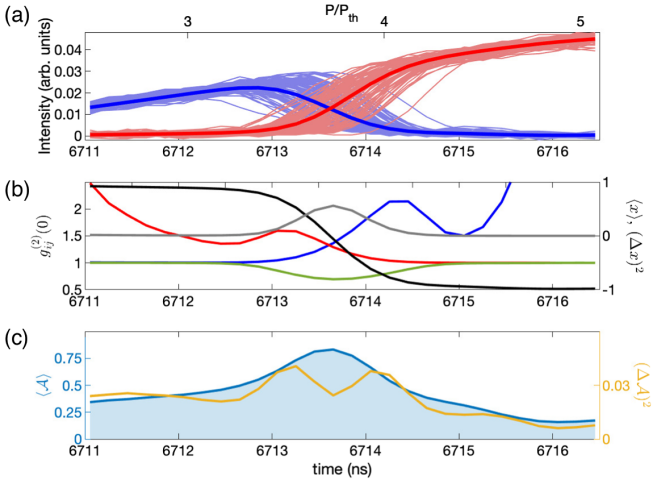

FIG. 2. Experimental time traces as the pump power is ramped up. (a) Intensity traces for B (blue) and A (red) modes measured with two APD detectors. Pump ramp duration = 6 ns. Thick lines: average corresponding to 10^4 time traces. (b) Second order correlations (left axis): $g^{(2)}_{BB}(0)$ (blue), $g^{(2)}_{AA}(0)$ (red) and $g^{(2)}_{BA}(0)$ (green); moments of the mode population imbalance [$\langle x \rangle$ (black) and $(\Delta x)^2$ (grey)] computed using the full statistics (right axis). (c) Two first moments of the order parameter $\mathcal{A}$: mean value $\langle \mathcal{A} \rangle$ (blue, left axis) and variance $(\Delta\mathcal{A})^2$ (yellow, right axis).

presents a maximum at the mode switching point, but its value is smaller, $\langle \mathcal{A} \rangle \approx 0.8$, and the pumping range for nonzero $\langle \mathcal{A} \rangle$ is broadened with respect to the macroscopic case. This last point is important since the nanolaser regime enhances the pumping interval of existence of the limit cycle. Note that the statistics of x and hence of $\mathcal{A}$ can be obtained through the statistics of I_B and I_A, which we will experimentally characterize hereafter.

Figure 2(a) shows the experimental time traces of the two eigenmodes detected in the far field in such a way that their emission can be spatially separated. Mode intensities are then simultaneously measured using two 550 MHz APD photodetectors as the pump power is ramped up. The time series have been used to reconstruct the statistics of the mode population imbalance [Fig. 2(b), right axis]. It can be observed that $\langle x \rangle$ has a steplike variation with a zero crossing that we refer to as the switching point, P_s. The full statistics of x can be used to compute the statistics of $\mathcal{A}$. In Fig. 2(c), we show the mean value $\langle \mathcal{A} \rangle$ together with the variance $(\Delta\mathcal{A})^2$. We observe a maximum of $\langle \mathcal{A} \rangle \approx 0.83$ at the switching point, in good agreement with the Langevin semiclassical predictions [Fig. 1(f)]. In addition, there is a peak of $(\Delta\mathcal{A})^2$ at each side of the switching point, also in agreement with the model. These statistical features are indicators of the emergence of a limit cycle, even though the direct measurement of cavity intensity time oscillations cannot be done due to the extremely high oscillation frequency together with the weak (sub-μW) output signals.

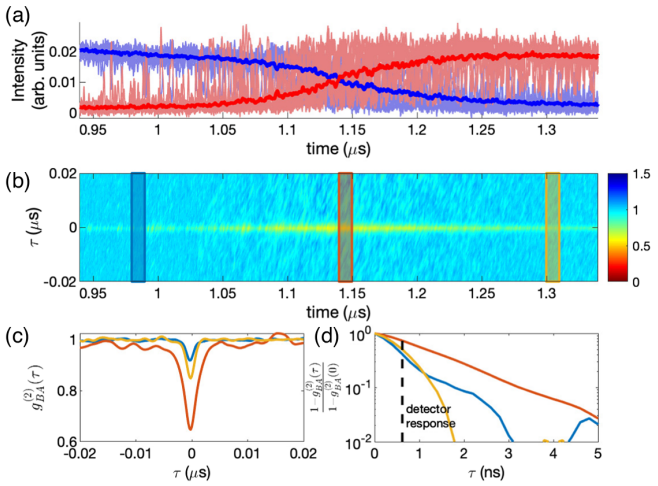

FIG. 3. Experimental time-resolved cross-correlation around a mode switching transition. (a) Time traces of B (blue) and A (red) modes (thick lines: average over 100 plateaus). The switching is induced by a slow thermal drift. (b) Time dependent correlations $g^{(2)}_{BA}(t,\tau)$; the regions before, near, and after the switching point are framed in blue, red, and yellow, respectively. (c) Average of $g^{(2)}_{BA}(t,\tau)$ over t within the boxes of (b). (d) Blowup of the normalized cross-correlation for positive τ.

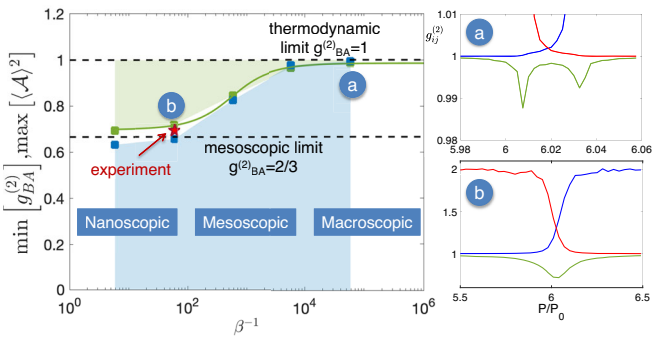

FIG. 4. Minimum of cross-correlations (green) and maximum of the squared mean limit cycle amplitude (blue squares) between eigenmodes of a laser dimer for increasing system size β^{-1}. Green line: guide to the eye. Right column: zero time delay intensity correlations $g^{(2)}_{ij}$ [$(i,j)=(B,B)$: blue, (A,A): red, and (B,A): green lines] as a function of the pump around the mode switching point, showing a double dip in the macroscopic regime (a) and a single dip in the mesoscopic regime (b). Red symbol: experimental result.

The dynamics become extremely slow at the switching point, allowing us to resolve the intensity fluctuations with our detectors (rise time = 620 ps). This is shown in the time resolved correlation measurements of Fig. 3, where the pump is a 100-period square waveform (peak power = 690 μW, duration = 1 μs, repetition rate = 100 kHz). We observe that the system slowly drifts, inducing a mode switching at $t \sim 1.14$ μs. This drift can be attributed to thermal effects whose timescale is 1 μs, i.e., much slower compared to the dynamical phenomena in play. Its quasistatic character allows us to resolve the correlation functions in time delay [τ, Fig. 3(b)]. We observe that, before and after the switching point, the duration of the cross-correlation dip is limited by the detector response [Figs. 3(c) and 3(d)]. However, the correlation decay time at the switching point is much longer (1.4 ns). Such a factor ~3 difference is a lower bound. We have confirmed this by numerical simulations that show a slowing down of more than one order of magnitude (Sec. III, Supplemental Material [26]). In the limit of very strong coupling, such a critical slowing down can also be observed in the spectrum of a 1D Fokker-Planck equation (Sec. VI, Supplemental Material [26]).

Usually, the experimentally accessible quantity is the photon correlation rather than the order parameter. Nevertheless, both of them are related. The zero time delay mode cross-correlations, $g^{(2)}_{BA}(\tau=0)$, can be easily deduced from the two lowest order moments of x. Under the hypothesis of decorrelated total intensity $I = I_B + I_A$ and x fluctuations, $\langle Ix\rangle = \langle I\rangle\langle x\rangle$, it can be shown that

$$g^{(2)}_{BA} = g^{(2)}_{II}\frac{1-\langle x^2\rangle}{1-\langle x\rangle^2}, \tag{4}$$

where we have removed $\tau = 0$ to simplify the notation. We will further assume that the total intensity fluctuations are Poissonian; hence $g^{(2)}_{II} = 1$, in agreement with our measurements (see Fig. S2, Supplemental Material [26]). The probability distribution of x is flat in the mesoscopic limit (Secs. I and V, Supplemental Material [26]) leading to $\langle x\rangle = 0$ and $\langle x^2\rangle = 1/3$; hence $g^{(2)}_{BA} = 2/3$, which can be interpreted as the mesoscopic limit. This theoretical prediction is also in good agreement with our experimental results. In Fig. 2(b) (left axis), we show $g^{(2)}_{AA}$, $g^{(2)}_{BB}$, and $g^{(2)}_{BA}$. Note that $g^{(2)}_{BA} \approx 0.7$ is less than unity at the switching point, revealing mode anticorrelations. These measurements have been confirmed using 50 ps resolution single nanowire single photon detectors in the pulsed pump regime (Sec. II, Supplemental Material [26]).

The mode cross-correlation minimum, $\min[g^{(2)}_{BA}]$, is strongly influenced by noise. In Fig. 4, we display numerical simulations decreasing the system size from $\beta^{-1} = 5.9\times10^4$ to 5.9, showing a clear crossover between the macroscopic and the mesoscopic regimes. Interestingly, the cross-correlation functions have a double dip structure in the macroscopic regime, whereas there is a single dip in the mesoscopic regime, in particular for $\beta = 0.017$ corresponding to our experimental situation.

The cross-correlation is related to the limit cycle amplitude as $\langle\mathcal{A}^2\rangle \approx g^{(2)}_{BA}$ at the switching point [Eq. (4)]. In addition, neglecting limit cycle amplitude fluctuations, we easily get $\langle\mathcal{A}\rangle \approx \sqrt{g^{(2)}_{BA}}$; both are shown in Fig. 4 for comparison. We point out that $g^{(2)}_{BA} = 1$ corresponds to the uncorrelated limit; hence the nontrivial statistical

information is contained in the cross-correlation depth (green area in Fig. 4). Since such features are vanishingly small in the thermodynamic limit [see Fig. 4(a)], they would most likely be hidden by noise, and no significant statistical information could be extracted in the macroscopic regime. In contrast, $g^{(2)}_{AB}$ is substantially less than one in the mesoscopic regime, thus becoming a good statistical indicator. Small modal cross-correlations have already been reported in other photonic systems such as VCSELs ([32,33] and Sec. V of [26]) or micropillar lasers ([34] and Sec. V of [26]), but no limit cycle dynamics have been reported in those examples.

In conclusion, we have shown that mode beating limit cycles emerge at the mode switching of a nanolaser dimer. This has been possible thanks to photon statistics measurements, which allowed us to compute the oscillation amplitude ($\mathcal{A}$). A maximum of $\langle\mathcal{A}\rangle$ is observed at the switching point, together with two maxima of $\Delta\mathcal{A}$ at each side of the transition, which are signatures of limit cycle bifurcations in the presence of noise, as predicted by a Langevin semiclassical model. We have shown that the limit cycle finite lifetime is due to its phase diffusion. However, while (field) phase diffusion in a laser can be explained as a Hopf bifurcation with additive noise leading to a Schawlow-Townes mechanism, in our case the specific nature of the noise and how it enters into the dynamical equations might result in a strong departure from such a theory. We conjecture, though, that our scenario may support vanishing eigenvalues of the Liouvillian with a nonzero imaginary part within a quantum master equation description [4,35]. In addition, we have related the order parameter to photon correlation measurements and showed that mesoscopic limit cycles are associated with a $2/3$ limit of the mode cross-correlations. Therefore, a coupled nanolaser system proves useful as a test bed for the investigation of limit cycles subjected to quantum noise and the spontaneous breaking of time translation symmetry.

We acknowledge discussions with A. Biella, Z. Denis, C. Ciuti, and M. Schirò. This work has been partially funded by the "Investissements d'Avenir" program (Labex NanoSaclay, ANR-10-LABX-0035), the Chateaubriand fellowship program, the ANR UNIQ DS078, DARPA DSO NLM, MINECO MOVELIGHT (PGC2018-099637-B-100 AEI/FEDER UE) and the H2020-FET-OPEN ChipAI projects.

*Corresponding author.
alejandro.giacomotti@c2n.upsaclay.fr
†Present address: Université Côte d'Azur, CNRS, Institut de Physique de Nice, F-06560 Valbonne, France.
‡Also at Université Paris Diderot, Sorbonne Paris Cité, 73013 Paris, France.

[1] J. Guckenheimer and P. Holmes, *Nonlinear Oscillations, Dynamical Systems, and Bifurcations of Vector Fields* (Springer-Verlag, New York, 1986).
[2] F. Wilczek, Phys. Rev. Lett. **109**, 160401 (2012).
[3] K. Sacha and J. Zakrzewski, Rep. Prog. Phys. **81**, 016401 (2018).
[4] F. Iemini, A. Russomanno, J. Keeling, M. Schirò, M. Dalmonte, and R. Fazio, Phys. Rev. Lett. **121**, 035301 (2018).
[5] V. DeGiorgio and M. O. Scully, Phys. Rev. A **2**, 1170 (1970).
[6] R. Graham and H. Haken, Z. Phys. A **237**, 31 (1970).
[7] R. Graham, Macroscopic potentials, bifurcations, and noise in dissipative systems, in *Noise in Nonlinear Dynamical Systems*, Vol. 1, edited by F. Moss and P. V. E. McClintock (Cambridge University Press, New York, 1989), pp. 225–278.
[8] P. R. Rice and H. J. Carmichael, Phys. Rev. A **50**, 4318 (1994).
[9] M. O. Scully and M. S. Zubairy, Quantum theory of the laser—density operator approach, in *Quantum Optics* (Cambridge University Press, New York, 1997), pp. 327–361.
[10] F. Minganti, A. Biella, N. Bartolo, and C. Ciuti, Phys. Rev. A **98**, 042118 (2018).
[11] E. Altman, L. M. Sieberer, L. Chen, S. Diehl, and J. Toner, Phys. Rev. X **5**, 011017 (2015).
[12] M. Wouters and I. Carusotto, Phys. Rev. B **74**, 245316 (2006).
[13] M. Ludwig and F. Marquardt, Phys. Rev. Lett. **111**, 073603 (2013).
[14] M. Schiró, C. Joshi, M. Bordyuh, R. Fazio, J. Keeling, and H. E. Türeci, Phys. Rev. Lett. **116**, 143603 (2016).
[15] J. Jin, D. Rossini, R. Fazio, M. Leib, and M. J. Hartmann, Phys. Rev. Lett. **110**, 163605 (2013).
[16] N. C. Zambon, S. R. K. Rodriguez, A. Lemaitre, A. Harouri, L. L. Gratiet, I. Sagnes, P. St-Jean, S. Ravets, A. Amo, and J. Bloch, arXiv:1911.02816.
[17] S. Kim, Y. G. Rubo, T. C. H. Liew, S. Brodbeck, C. Schneider, S. Höfling, and H. Deng, Phys. Rev. B **101**, 085302 (2020).
[18] A. Giraldo, B. Krauskopf, N. G. R. Broderick, J. A. Levenson, and A. M. Yacomotti, New J. Phys. **22**, 043009 (2020).
[19] P. Hamel, S. Haddadi, F. Raineri, P. Monnier, G. Beaudoin, I. Sagnes, A. Levenson, and A. M. Yacomotti, Nat. Photonics **9**, 311 (2015).
[20] S. S. Deka, S. H. Pan, Q. Gu, Y. Fainman, and A. E. Amili, Opt. Lett. **42**, 4760 (2017).
[21] M. Marconi, J. Javaloyes, P. Hamel, F. Raineri, A. Levenson, and A. M. Yacomotti, Phys. Rev. X **8**, 011013 (2018).
[22] M. Marconi, J. Javaloyes, F. Raineri, J. A. Levenson, and A. M. Yacomotti, Opt. Lett. **41**, 5628 (2016).
[23] N. Takemura, M. Takiguchi, and M. Notomi, arXiv:1904.01743.
[24] T. Wang, G. P. Puccioni, and G. L. Lippi, Sci. Rep. **5**, 15858 (2015).
[25] Y. Yamamoto, S. Machida, and G. Björk, Phys. Rev. A **44**, 657 (1991).
[26] See Supplemental Material at http://link.aps.org/supplemental/10.1103/PhysRevLett.124.213602 for additional experimental and theoretical information, which also includes Refs. [27–31].

[27] M. B. Willemsen, M. P. van Exter, and J. P. Woerdman, Phys. Rev. A **60**, 4105 (1999).
[28] M. Sondermann, M. Weinkath, T. Ackemann, J. Mulet, and S. Balle, Phys. Rev. A **68**, 033822 (2003).
[29] H. A. M. Leymann, C. Hopfmann, F. Albert, A. Foerster, M. Khanbekyan, C. Schneider, S. Höfling, A. Forchel, M. Kamp, J. Wiersig, and S. Reitzenstein, Phys. Rev. A **87**, 053819 (2013).
[30] C. Redlich, B. Lingnau, S. Holzinger, E. Schlottmann, S. Kreinberg, C. Schneider, M. Kamp, S. Höfling, J. Wolters, S. Reitzenstein *et al.*, New J. Phys. **18**, 063011 (2016).
[31] S. Holzinger, C. Redlich, B. Lingnau, M. Schmidt, M. von Helversen, J. Beyer, C. Schneider, M. Kamp, S. Höfling, K. Lüdge, X. Porte, and S. Reitzenstein, Opt. Express **26**, 22457 (2018).
[32] E. L. Blansett, M. G. Raymer, G. Cui, G. Khitrova, H. M. Gibbs, D. K. Serkland, A. A. Allerman, and K. M. Geib, IEEE J. Quantum Electron. **41**, 287 (2005).
[33] F. Prati, G. Giacomelli, and F. Marin, Phys. Rev. A **62**, 033810 (2000).
[34] H. A. M. Leymann, D. Vorberg, T. Lettau, C. Hopfmann, C. Schneider, M. Kamp, S. Höfling, R. Ketzmerick, J. Wiersig, S. Reitzenstein, and A. Eckardt, Phys. Rev. X **7**, 021045 (2017).
[35] K. Seibold, R. Rota, and V. Savona, Phys. Rev. A **101**, 033839 (2020).